

Electronic supplementary information (ESI) for the manuscript:

Light-assisted O-methylation of Phenol with Dimethyl Carbonate
over Layered Double Oxide Catalyst

Xiaoyu Wang,^{a,b} Ruiyi Wang,^{*a} Xianmo Gu,^a Jianfeng Jia^c and Zhanfeng Zheng^{*a,b}

^a *State Key Laboratory of Coal Conversion, Institute of Coal Chemistry, Chinese Academy of Sciences, Taiyuan, Shanxi 030001, China*

^b *Center of Materials Science and Optoelectronics Engineering, University of Chinese Academy of Sciences, Beijing 100049, PR China*

^c *The School of Chemical and Material Science, Shanxi Normal University, Linfen, Shanxi 041004, PR China*

Experimental Section

Preparation of Catalysts: Layered double hydroxides was prepared using a sol-gel process following established procedures with some modification,^{1,2} which were denoted as MgAl-LDHs, ZnAl-LDHs, and NiAl-LDHs. Then the LDHs was calcined at 450 °C (heating rate 10 °C/min) in dry air for 8 h, yielding mixed oxides, which were denoted as MgAl-LDO, ZnAl-LDO, and NiAl-LDO. For convenience, catalysts were designated as Mg₁Al-LDO, Mg₂Al-LDO, Mg₃Al-LDO, Zn₃Al-LDO, and Ni₃Al-LDO when Mg/Al atomic ratios were 1, 2, 3 and Zn/Al, Ni/Al atomic ratios were 3, respectively.

Characterization of Catalysts: Powder X-ray diffraction (XRD) spectroscopy was performed on a Bruker D8 Advanced diffractometer operating with Cu K α radiation ($\lambda = 1.5405 \text{ \AA}$). The nitrogen sorption isotherms were measured at -196 °C on a TriStar II 3020 volumetric adsorption analyzer. Prior to the measurement, all the samples were degassed under evacuation at 150 °C for 10 h. The surface area was calculated from the adsorption branch by the Brunauer-Emmett-Teller (BET) method and the pore size distribution was obtained by desorption isotherms using the Barret-Joyner-Halender (BJH) method. Acidity and basicity measurements are carried out by TPD of NH₃ and CO₂, respectively. Typically about 100 mg of the catalyst is secured between quartz wool plugs in the micro-reactor, pre-treated in nitrogen at 200 °C for 1 h and then cooled to 50 °C prior to the adsorption of NH₃ or CO₂ at this temperature. After the adsorption of NH₃ or CO₂ (30 ml/min) for 30 min, the catalyst is flushed with nitrogen for 60 min at 50 °C to remove the physisorbed gas from the surface of the catalyst. The desorption pattern has been recorded at a heating ramp of 10 °C/min from 50 to 800 °C using a recorder connected to a GC equipped with a TCD detector. Raman spectroscopy was performed using a Horiba LabRAM HR800 spectrometer. Thermogravimetric/differential thermal (TG/DTA) analysis was carried out on a Rigaku TG in air with a heating rate of 10 °C/min and 100 mg of sample were used. Fourier transform infrared spectroscopy (FTIR) was performed using a Nicolet Magna-IR 550-II spectrometer with KBr pellets. The UV-vis diffuse reflectance spectra (DRS) were observed on a Shimadzu UV-3600 UV-vis-NIR spectrophotometer.

Catalytic Reactions: The catalytic reactions were carried out in a 100 mL stainless steel autoclave equipped with a magnetic stirrer in an argon atmosphere. In a typical experiment, reactants and catalyst were introduced and then the reaction was performed at the required temperature under autogenous pressure using a 500 W super-pressure mercury lamp as the light source. The products were analyzed using a Shimadzu 2014C GC equipped with a WondaCap 5 column after centrifugal separation from the catalysts. The identity of the products was established by the comparison of retention times of authentic samples and also by GC-MS.

In order to strictly avoid exposure of the reaction to light, the stainless steel autoclave was sheltered with aluminum foil. The reaction temperature under irradiation was maintained the same as the reaction in the dark to make sure that the comparison is meaningful.

Calation details of activation energy: The values of the slopes calculated from the kinetic plots, as shown in Fig. 1b, are equal to the value of the rate constant k . According to the Arrhenius equation, two straight lines of $\ln k$ versus $(1/T)$ were obtained, from which the activation energies of photocatalytic reaction and O-methylation of phenol (in the dark) could be derived as the value of the slope is $-E_a/R$. Then the activation energies of light-driven (denoted as E_{ap}) and thermal-driven (denoted as E_{ad}) reaction were calculated according to the Arrhenius equation, as shown in Fig. 1b, being 106.58 and 97.55 kJ/mol respectively. From these results, which means that 9.03 kJ/mol ($\Delta E_a = E_{ad} - E_{ap}$) is reduced by irradiation.

More Characterization Results

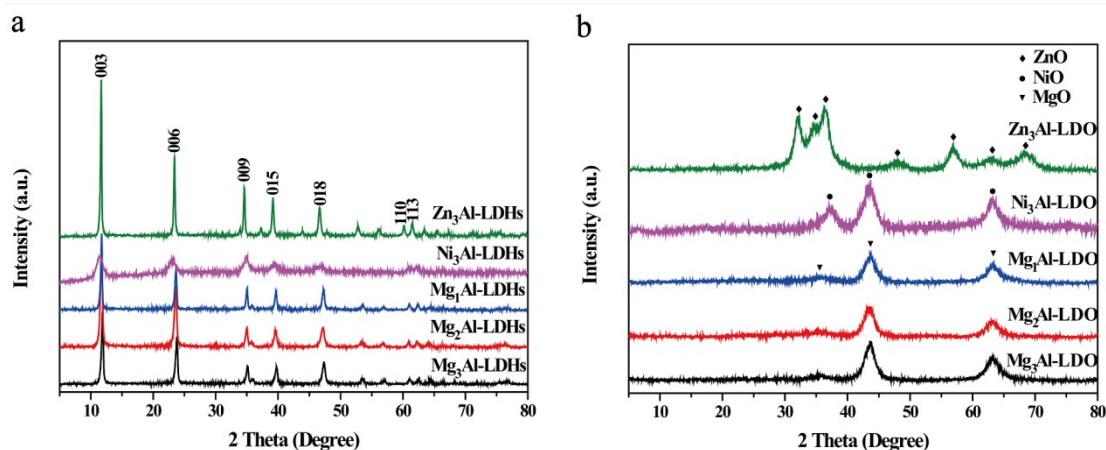


Fig. S1 XRD patterns of the samples: (a) LDHs and (b) LDO.

Table S1 Physical characteristics of samples.

Catalyst	$S_{\text{BET}}(\text{m}^2/\text{g})^{\text{a}}$	$V_{\text{P}}(\text{cm}^3/\text{g})^{\text{b}}$	$D_{\text{P}}(\text{nm})^{\text{c}}$	mmol basic sites per g	mmol acid sites per g
Mg ₃ Al-LDO	187.680	0.283	6.025	2.25	1.10
Mg ₂ Al-LDO	52.156	0.294	22.520	2.13	0.96
Mg ₁ Al-LDO	125.397	0.322	10.276	2.09	0.88
Zn ₃ Al-LDO	187.900	0.277	5.907	1.98	0.50
Ni ₃ Al-LDO	266.291	1.187	17.831	2.07	0.79
Mg ₃ Al-LDHs ^d	33.724	0.142	16.790	---	---
MgO	38.524	0.184	19.116	2.70	0.40
Al ₂ O ₃	251.351	0.446	7.103	1.35	1.69

a. Specific surface area; b. Total pore volume; c. Average pore diameter; d. TPD results are unreliable for MgAl-LDHs due to it will gradually releases H₂O and CO₂ as the reaction temperature rise.

Discussion:

XRD patterns of the as-synthesized LDHs samples are shown in Fig. S1a, which exhibit a hydrotaalcite-like structure similar to the previous literature with intense sharp and symmetric peaks for (003), (006), (009), (015), (018), (110) and (113) planes.¹ The layered double oxide also exhibited the typical XRD patterns of the corresponding oxides structure (Fig. S1b), which is well consistent with the reported data (JCPDS No. 45-0946 for MgAl-LDO, JCPDS No. 36-1451 for ZnAl-LDO and JCPDS No. 44-1159 for NiAl-LDO). The physico-chemical characteristics of catalysts are presented in Table S1. The specific surface area of the catalysts shows less obvious regularity. NH₃ and CO₂ up-take of the catalysts shows the presence of basicity and acidity of different strengths in Table S1 and is found to be very high in MgAl-LDO samples. The total basicity per g of the catalysts showed the following order: MgO > Mg₃Al-LDO > Mg₂Al-LDO > Mg₁Al-LDO > Ni₃Al-LDO > Zn₃Al-LDO > Al₂O₃, the

acidity in the following order: $\text{Al}_2\text{O}_3 > \text{Mg}_3\text{Al-LDO} > \text{Mg}_2\text{Al-LDO} > \text{Mg}_1\text{Al-LDO} > \text{Ni}_3\text{Al-LDO} > \text{Zn}_3\text{Al-LDO} > \text{MgO}$.

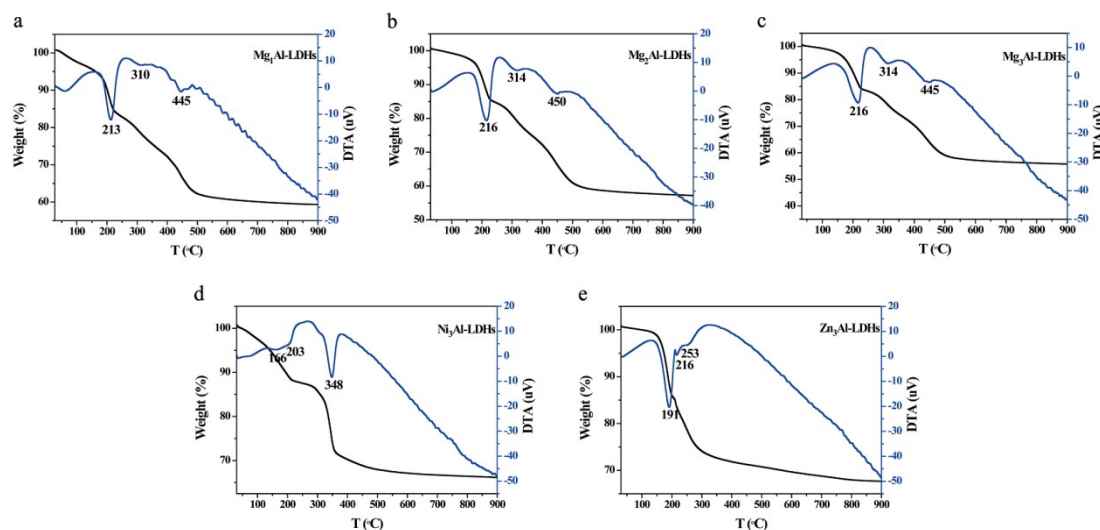


Fig. S2 TG-DTA curves of LDHs samples: (a) $\text{Mg}_1\text{Al-LDHs}$, (b) $\text{Mg}_2\text{Al-LDHs}$, (c) $\text{Mg}_3\text{Al-LDHs}$, (d) $\text{Ni}_3\text{Al-LDHs}$, and (e) $\text{Zn}_3\text{Al-LDHs}$.

Discussion:

The TG-DTA curves of five LDHs samples are displayed in Fig. S2. For MgAl-LDHs samples (Fig. S2a, S2b, S2c), the first endothermic peak, due to the dehydration of interlayer water, was observed at 213 °C for $\text{Mg}_1\text{Al-LDHs}$, at 216 °C for $\text{Mg}_2\text{Al-LDHs}$ and $\text{Mg}_3\text{Al-LDHs}$, The second peak appeared at 310 °C for $\text{Mg}_1\text{Al-LDHs}$, at 314 °C for $\text{Mg}_2\text{Al-LDHs}$ and $\text{Mg}_3\text{Al-LDHs}$; the third at 445 °C for $\text{Mg}_1\text{Al-LDHs}$ and $\text{Mg}_3\text{Al-LDHs}$, at 450 °C for $\text{Mg}_2\text{Al-LDHs}$. The second peak is attributed to the dehydroxylation of OH bound with Al, and the third peak is ascribed to the dehydroxylation of OH bound with Mg and the main CO_2 evolution. Three weight loss steps were observed in the TG-DTA curves for all MgAl-LDHs samples.³ For $\text{Ni}_3\text{Al-LDHs}$ (Fig. S2d), the first endothermic effect was associated with H_2O evolution and corresponded to a release of interlayer water at 166 °C and 203 °C. The second endothermic effect was accompanied by simultaneous H_2O and CO_2 evolution associated with dehydroxylation of hydroxide layers and decomposition of interlayer carbonate at 348 °C.⁴ For $\text{Zn}_3\text{Al-LDHs}$ (Fig. S2e), the first endothermic peak at 191 °C, accompanied by a shoulder around 216 °C, could be ascribed to the dehydration of interlayer water; the second endothermic peak at 253 °C could be contributed to the dehydroxylation of the metal hydroxide layers of $\text{Zn}_3\text{Al-LDHs}$.⁵ It is concluded that the structure can remain thermal stability when calcinated at 450 °C for $\text{Mg}_1\text{Al-LDHs}$, $\text{Mg}_2\text{Al-LDHs}$ and $\text{Mg}_3\text{Al-LDHs}$, at 350 °C for $\text{Ni}_3\text{Al-LDHs}$ and at 260 °C for $\text{Zn}_3\text{Al-LDHs}$. Thus choose the 450 °C as the optimum calcination temperature for all samples.

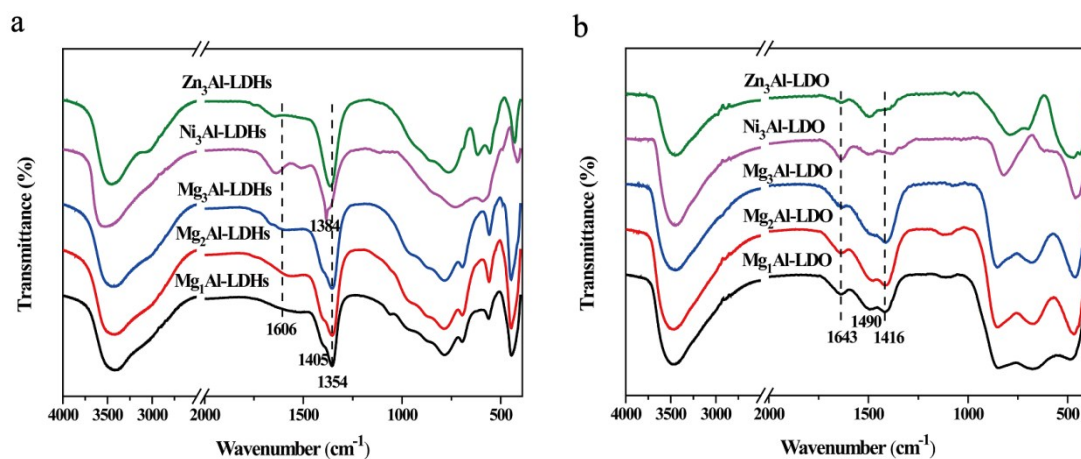


Fig. S3 FT-IR spectra of samples: (a) LDHs and (b) LDO.

Discussion:

The FT-IR spectra of LDHs samples are shown in Fig. S3a. The broad band centred around 3500 cm^{-1} is assigned to a complex of overlapping stretching modes of the hydroxyl groups present in the brucite-type layer and the interlayer water molecules. The band at 1606 cm^{-1} is associated with the deformation mode of the hydroxyl groups. The bands at 1354 cm^{-1} and 1405 cm^{-1} are assigned to the carbonate species antisymmetric stretching modes. Several bands below 1000 cm^{-1} are associated with the M-O vibrational modes (Mg-O, Al-O) in the brucite-type layer.⁶ Most of $\text{Ni}_3\text{Al-LDHs}$ bands are similar to the bands of MgAl-LDHs samples besides the band at 1384 cm^{-1} , which assigned to nitrate antisymmetric stretching vibration.⁶ Because the nitrate ions incorporated into the hydrotalcite interlayer along with the carbonate and water species in $\text{Ni}_3\text{Al-LDHs}$ sample. And all bands of $\text{Zn}_3\text{Al-LDHs}$ are similar to the bands of MgAl-LDHs samples. Among the FT-IR spectra of all LDHs samples, the band intensity of $\text{Ni}_3\text{Al-LDHs}$ is the lowest. A comparison of the results of infrared spectra shows good agreement with the XRD results (Fig. S1a) which shows the lowest crystallinity of $\text{Ni}_3\text{Al-LDHs}$, an decrease in order crystallinity along with the decrease in intensity and increases in band width in the infrared spectra.⁶

As show in Fig. S3b, after calcinated at $450\text{ }^\circ\text{C}$, all the bands of hydroxyl groups and carbonate species decrease in intensity and high frequency shift ascribed to the desorption of H_2O and CO_2 of LDHs with in the thermal treatment, which shows good agreement with the TG-DTA results (Fig. S2).

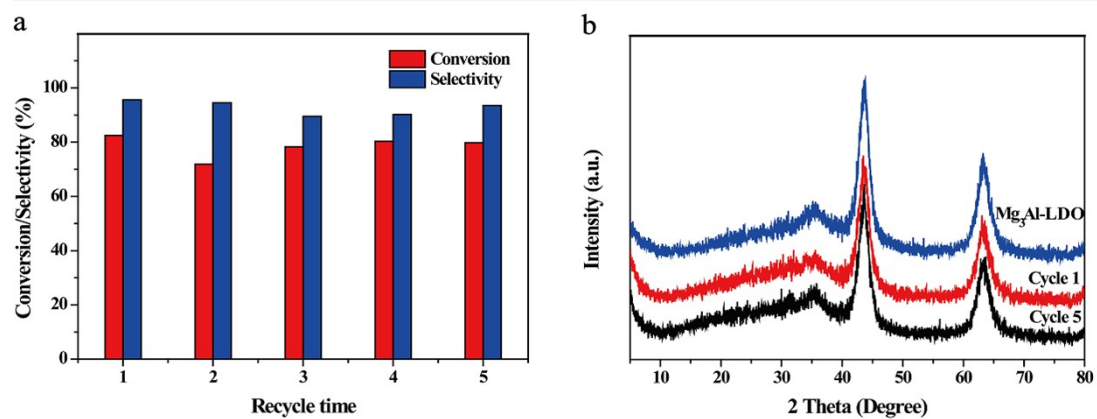


Fig. S4 (a) Recyclability of Mg₃Al-LDO in O-methylation of phenol for five cycles. (b) X-ray diffraction (XRD) patterns of the purified Mg₃Al-LDO and the Mg₃Al-LDO used after one time and five times.

Discussion:

The recyclability nature of catalyst are investigated in Fig. S4, Mg₃Al-LDO was successfully recovered by centrifugation and reused for five cycles without any appreciable loss in both relative activity and selectivity (Fig. S4a). It was found that there is no obvious structure change after the reaction according to the XRD patterns of the sample after 5 cycles (Fig. S4b).

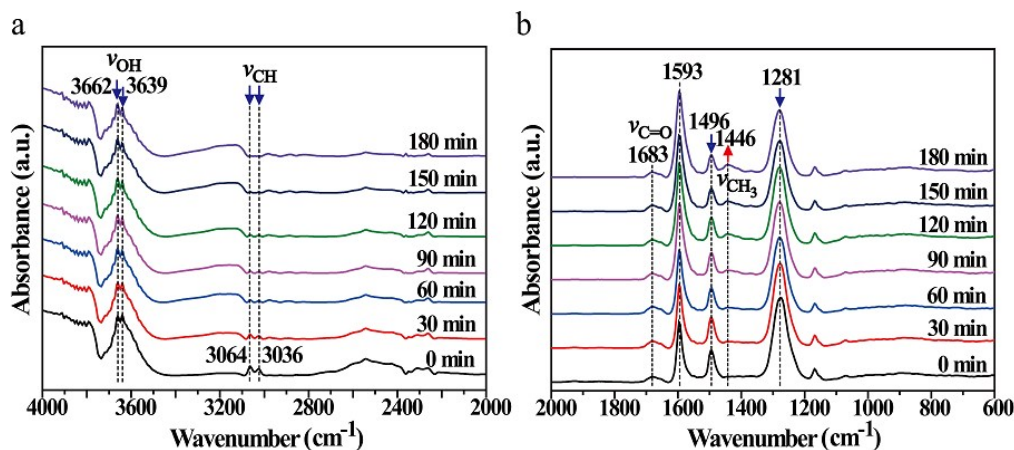


Fig. S5 In-situ FT-IR spectra of Mg_3Al -LDO after co-adsorption of phenol and DMC: (a) from 4000 cm^{-1} to 2000 cm^{-1} and (b) from 2000 cm^{-1} to 600 cm^{-1} (downward arrow: band intensity decreases with the time; upward arrow: band gradually appears with the time).

Discussion:

In-situ FT-IR spectra after coadsorption of phenol and DMC on Mg_3Al -LDO shown in Fig. S5. Band at 3662 cm^{-1} and 3639 cm^{-1} are typical bands of the O-H stretching vibrations of phenol, which proportionally diminished in intensity indicating that hydroxyl of phenol has been deprotonated.⁷ Bands at 3064 cm^{-1} and 3036 cm^{-1} are typical bands of the C-H stretching vibrations of the aromatic ring of phenol. Low frequency shift of this band compare to the neat phenol (3065 cm^{-1} , 3047 cm^{-1}) indicate the presence of perturbed OH groups which belong most likely to phenol H-bonded (of hydroxyl) to base sites of LDO. The intensive absorption band at 1496 cm^{-1} and 1593 cm^{-1} are assigned to the carbon-carbon double bond deformation vibrations of the aromatic ring.⁸ These bands are slightly displaced to lower wavenumbers as compared with phenol in CCl_4 solution where they occur at 1596 cm^{-1} and 1604 cm^{-1} . Band at 1281 cm^{-1} is ascribed to C-OH vibration of the ring. All these spectral features of phenol, except the band at 1593 cm^{-1} , remains about half of the original intensity in the range of the aromatic ring vibrations after co-adsorption of phenol and DMC at 180 min. Indicate that part of the phenol has desorbed, another part of the phenol was deprotonated.

Band at 1446 cm^{-1} is attributed to the asymmetric variable angle vibration of anisole methyl group which distinguish from the band at 1454 cm^{-1} ascribed to the vibration of DMC methyl groups. As the reaction proceeds, the band appeared from nothing and increased in intensity indicating the anisole production.

Band at 1683 cm^{-1} is attributed to the vibration of DMC carbonyl oxygen group.⁹ Low frequency shift of this band compared to the IR spectra of neat DMC ($1780\text{-}1680\text{ cm}^{-1}$) indicate the carbonyl oxygen atoms of DMC associated with the acid sites of LDO due to the coordination of carbonyl oxygen atoms with metal atoms can result in the bond length increasing. Distinguish from the blue shift of the C=O bond is expected with respect to

neat DMC if the ester oxygen atoms of DMC associated the acid sites of LDO.

Table S2 Concentrations of base and acid site according to CO₂-TPD and NH₃-TPD profiles.

Catalyst	basic sites (mmol/g)			acid sites (mmol/g)			
	B _{TOTAL} ^a	B _M ^b	B _S ^b	A _{TOTAL} ^c	A _W ^d	A _M ^d	A _S ^d
Mg ₃ Al-LDO	2.25	1.50	0.75	1.10	0.10	0.71	0.29
Ni ₃ Al-LDO	2.07	1.20	0.87	0.79	0.28	0.31	0.20
Zn ₃ Al-LDO	1.98	1.14	0.84	0.50	0.16	0.19	0.15

a. B_{TOTAL} is the total concentration of base sites calculated based on CO₂-TPD. b. B_M and B_S represent the concentration of medium and strong base site, respectively. c. A_{TOTAL} is the total concentration of acid sites calculated based on NH₃-TPD. d. A_W, A_M, and A_S denote the concentration of weak, medium, and strong acid site, respectively.

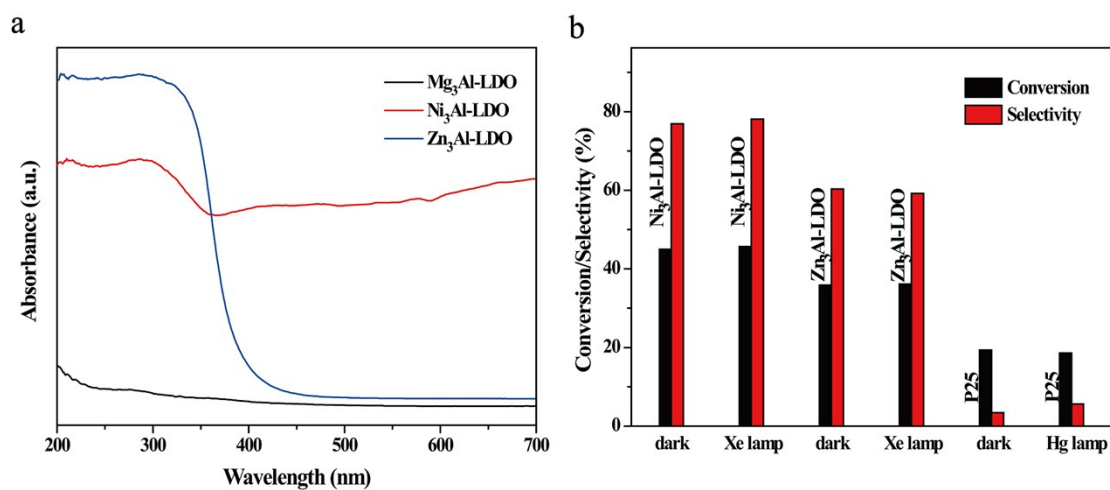


Fig. S6 (a) UV-Vis spectra of Mg₃Al-LDO, Ni₃Al-LDO, and Zn₃Al-LDO. (b) Conversion rates of DMC and selectivities for anisole using Ni₃Al-LDO and Zn₃Al-LDO as catalysts under full-spectrum Xe lamp, using TiO₂-P25 under high-pressure mercury lamp and in the dark. Reaction conditions: catalyst, 0.28 g; phenol, 135 mmol; DMC, 67.5 mmol; Ar, 1 atm; light intensity, 66 mW/cm² (Xe lamp, 100 mW/cm²); reaction temperature, 160 °C; reaction time, 6 h.

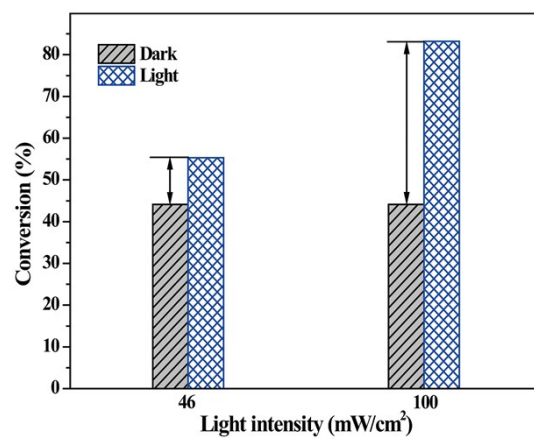


Fig. S7 Dependence of the catalytic activity of $\text{Mg}_3\text{Al-LDO}$ catalyst for O-methylation of phenol on the intensity of high-pressure mercury lamp irradiation. Reaction conditions: catalyst, 0.28 g; phenol, 135 mmol; DMC, 67.5 mmol; Ar, 1 atm; reaction temperature, 160 °C; reaction time, 6 h.

Table S3 The amount of methanol and CO₂ generated during reaction and the carbon balance of reaction.

Catalyst		Conv	Sel.	n _{anisole}	n _{methanol}	n _{CO2}	Carbon balance
		(%)	(%)	(mmol)	(mmol)	(mmol)	(%)
Mg ₃ Al-LDO	light	82.5	95.6	53.2	55.4	53.2	99.4
	Dark	44.1	79.5	23.7	26.8	25.1	98.4
Ni ₃ Al-LDO	light	56.3	88.4	33.6	33.3	30.0	96.9
	Dark	45.0	76.9	23.4	25.8	24.3	97.7
Zn ₃ Al-LDO	light	47.2	69.7	22.2	29.5	25.7	98.7
	Dark	35.9	60.3	14.6	18.2	16.9	96.2

Reaction conditions: catalyst, 0.28 g; phenol, 135 mmol; DMC, 67.5 mmol; Ar, 1 atm; light intensity (high-pressure mercury lamp), 66 mW/cm²; reaction temperature, 160 °C; reaction time, 6 h.

Notes and references

- 1 Y. Zhao, Y. Zhao, G. I. N. Waterhouse, L. Zheng, X. Z. Cao, F. Teng, L. Z. Wu, C. H. Tung, D. O'Hare and T. Zhang, *Adv. Mater.*, 2017, 1703828-1703837.
- 2 J. B. Han, J. Lu., M. Wei, Z. L. Wang and X. Duan, *Chem. Commun.*, 2008, 5188-5190.
- 3 T. Hibino, Y. Yamashita, K. Kosuge and A. Tsunashima, *Clay. Clay. Mine.*, 1995, **43**, 427-432.
- 4 F. Kovanda, T. Rojka, P. Bezdicka, K. Jiratova, L. Obalova, K. Pacultova, Z. Bastl and T. Grygar, *J. Solid. State. Chem.*, 2009, **182**, 27-36.
- 5 K. Dutta, S. Das, A. Pramanik, *J. Colloid Interface Sci.*, 2012, **366**, 28-36.
- 6 L. Hickey, J. T. Kloprogge, R. L. Frost, *J. Mater. Sci.*, 2000, **35**, 4347-4355.
- 7 T. Ebata, T. Watanabe and N. Mikami, *J. Phys. Chem.*, 1995, **99**, 5761-5764.
- 8 E. B. Wilson, *Phys. Rev.*, 1934, **45**, 706-714.
- 9 J. S. Byrne, P. F. Jackson and K. J. Morgan, *Perkin Trans.*, 1975, **2**, 1800-1802.